VOLUME 7, NUMBER 4, APRIL 2007

NANO LETTERS

Charge Transport in Cellular Nanoparticle Networks: Meandering through Nanoscale Mazes

Matthew O. Blunt,[†] Milovan Šuvakov,[‡] Fabio Pulizzi,[†] Christopher P. Martin,[†] Emmanuelle Pauliac-Vaujour,[†] Andrew Stannard,[†] Andrew W. Rushforth,[†] Bosiljka Tadić,[‡] and Philip Moriarty*,[†]

The School of Physics and Astronomy, The University of Nottingham, Nottingham NG7 2RD, U.K., and Department of Theoretical Physics, Jožef Stefan Institute, Box 3000, SI-1001 Ljubljana, Slovenia

Received July 18, 2006; Revised Manuscript Received February 13, 2007

ABSTRACT

The transport of electrons through topologically complex two-dimensional Au nanoparticle networks has been investigated using a combination of low temperature (4.5 K) direct current *I*(*V*) measurements and numerical simulations. Intricate, spatially correlated nanostructured networks were formed via spin-casting. The topological complexity of the nanoparticle assemblies produces *I*(*V*) curves associated with nonlinearity exponents, $\zeta \sim 4.0$. Simulations based on tunneling transport in sparse and inhomogeneous planar networks are used to elucidate the influence of topology on the value of ζ.

Driven in part by key advances in assembly and fabrication techniques,[1−4] there has been significant progress made in our understanding of charge transport in both well-ordered and structurally disordered nanoparticle arrays of various dimensionalities.[5−11] In particular, a number of groups—foremost, that of Jaeger et al.[5,6,12,13]—have recently built on (and significantly extended) seminal theoretical work by Middleton and Wingreen (MW)[14] in the early 1990s to elucidate the mechanism of electron transfer through extended nanoparticle lattices. There has consequently been a strong focus on the synthesis of long-range ordered colloidal nanoparticle arrays, and remarkable breakthroughs in this area have recently been made by Bigioni et al.[2] who have shown that assembly at the solvent−air interface[3] can promote the formation of remarkably well-ordered monolayers.

Far-from-equilibrium self-organization at the solvent−substrate interface[15−21] produces a variety of intricate patterns which generally have a substantially lower degree of long-range order than those produced by controlling assembly at the air-exposed surface of the solvent droplet.[2,3] Nevertheless, these types of substrate-mediated out-of-equilibrium pattern have very many intriguing (and potentially technologically relevant) properties as compared to perfectly close-packed domains of nanocrystals. Specifically, in far-from-equilibrium assembly, the inherent length scales/correlation lengths of the self-organized system need not be dictated *solely* by interparticle interactions. That is, spatial correlations over a

[†] The School of Physics and Astronomy, The University of Nottingham.
[‡] Department of Theoretical Physics, Jožef Stefan Institute.

10.1021/nl061656e CCC: $37.00
Published on Web 03/03/2007

wide variety of length scales (nanometres, micrometers, and, potentially, millimeters) can be developed. Indeed, far-from-equilibrium self-organization makes *hierachical* or multiscale structuring of matter possible (as exploited for quite some time by the polymer community[22,23]).

In this Letter we report a combined experimental and computer simulation study of electron transport through topologically complex Au nanoparticle networks. A "non-disruptive" shadow masking technique was used to deposit electrical contacts on top of the nanoparticle assemblies, circumventing problems associated with variations in solvent wettability and nanoparticle mobility inherent in methods involving colloidal particle deposition onto prefabricated electrodes. The far-from-equilibrium spin-coating process generates arrays with a distribution of spatially correlated voids[20] which in turn yield a wide distribution of complex percolation pathways through the network. The $I(V)$ characteristics of the nanoparticle networks exhibit very high values ($\sim$4.0) of the scaling exponent ζ, as compared to $\zeta \sim 2.3$ measured for networks with low void fraction.[5] To elucidate the dependence of ζ on network topology, we model charge transport via a hybrid of the Rabani et al.[17] Ising model approach (to simulate pattern formation in nanoparticle assemblies) and the classic MW tunneling model.[14] A modified Rabani et al.[17] algorithm is used to generate network formation in nanoparticle arrays, producing patterns in good, *quantitative* agreement with those observed experimentally.[20]

The nanocrystals used in the experiments were thiol-passivated colloidal gold particles in toluene.[24] The mean particle size was determined from small-angle X-ray scattering measurements[21] for pentanethiol- and octanethiol-passivated particles. This was 1.90 and 1.84 nm, respectively (with a rather large σ of 0.16 nm in both cases). Nanoparticle assemblies were spin-cast (4 krpm, 30 s, 25 μL solution volume) from toluene onto 5 mm^2 pieces of silicon wafers coated with a 200 nm thick dielectric layer of thermally grown oxide. Prior to nanoparticle deposition the substrates were cleaned via ultrasonication in ethyl lactate, acetone, methanol, and isopropyl alcohol.

Electrical contacts were deposited on top of the nanocrystal arrays via shadow masking. The shadow masking technique was used to ensure that the spin-cast nanoparticle arrays were not disrupted via dewetting effects arising from physical heterogeneities (i.e., electrical contacts) on the substrate surface.[25] The shadow mask consisted of 200 μm wide slits across which 5 and 10 μm pieces of tungsten wire were stretched. By evaporation of gold through this mask, planar gold contacts with gap widths ranging between 0.5 and 10 μm could be formed (see Figure 1). Before and after the deposition of electrical contacts, the samples were characterized with tapping mode AFM imaging (using either a Digital Instruments Multimode AFM or an Asylum Research MFP-3D). Samples were then mounted on standard TO5 headers which in turn were placed in a liquid helium flow cryostat for variable temperature electrical measurements (4.5−80 K). All $I(V)$ data presented in this paper were, however, taken at 4.5 K. Direct current $I(V)$ curves were acquired between $\pm$20 V, with a current resolution of $\sim\pm$100 fA.

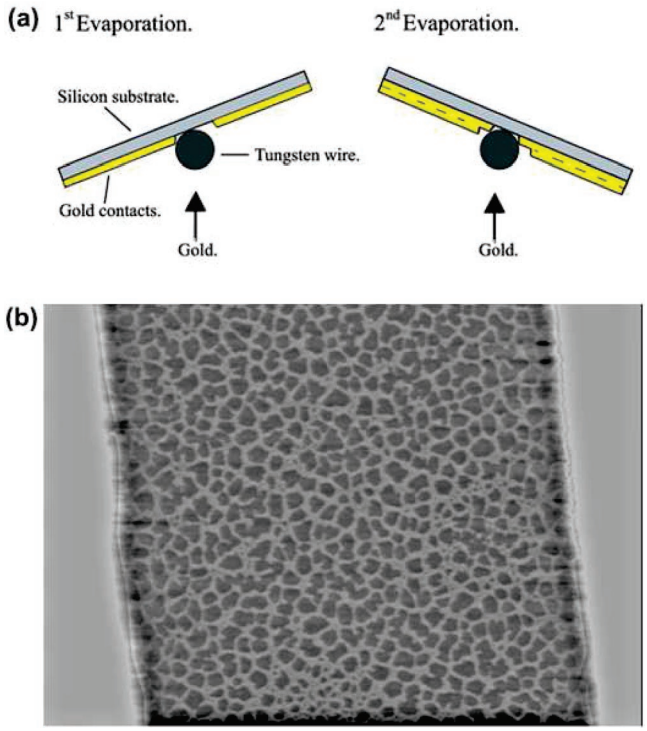

Figure 1. (a) Simple schematic illustration of a two-step shadow mask process used to fabricate electrical contacts on nanoparticle assemblies. (b) Contrast-enhanced (high pass filtered) tapping mode AFM image of a contacted submonolayer nanoparticle network comprising octanethiol-passivated Au nanoparticles between two gold electrodes having an edge-to-edge separation of $\sim$4 μm (cf. Figure 5a).

Spin-cast and drop-deposited nanocrystal assemblies form a broad range of striking patterns, spanning isolated droplets through bicontinuous "labyrinths" to cellular networks.[15−21,25,26] Here we focus only on cellular networks, an example of which is shown in Figure 1. A variety of morphological measures have previously been used[19,20] to show that the void positions are spatially correlated, unlike the random void distributions considered or postulated in previous work.[7,10]

The strategy used for numerical simulations of charge transport in cellular nanoparticle networks was as follows. First, the process of network formation (via solvent evaporation and diffusion of the interacting particles on the substrate) was simulated within a discrete model described by Rabani et al.[17] and Martin et al.[20] Depending on the parameters used in the model,[17,20,26] a variety of complex structures comprising inhomogeneous particle distributions and voids of different sizes emerge which closely match those observed experimentally (as measured by tesselation analysis and Minkowski morphometry[20]). A network, i.e., a mathematical graph consisting of nodes and links between nodes, is then constructed in the following way. The nodes are represented by nanoparticles on the substrate and links are inserted between pairs of nodes separated by distances smaller than a tunneling radius r.[27] In this way the sparse filling of the plane by particles leads to an inhomogeneous network with varying node connectivity (see Figure 2).

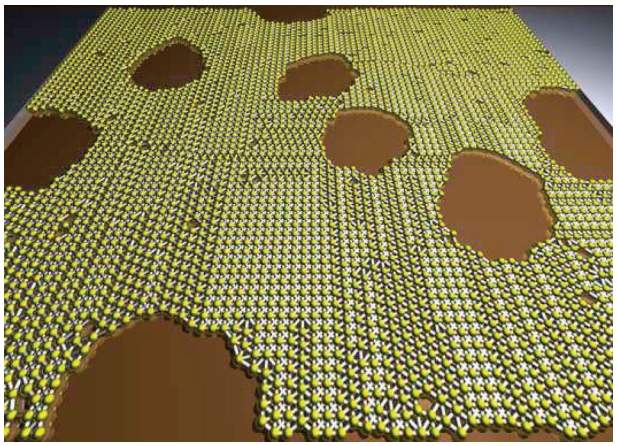

Figure 2. A three-dimensional rendering of a simulated nanoparticle network structure of the type used in the transport calculations.

To simulate numerically the conduction through these networks, we implement a microscopic model of single electron tunneling which works for any type of structure defined by the corresponding adjacency matrix $\hat{\mathbf{A}}$ (see ref 27). This is a generalization of the model put forward by Middleton and Wingreen[14] and extended by Parthasarathy et al.[5] Briefly, the electrostatic energy of charged particles on a network of N nodes is given by

$$E = \frac{1}{2}\mathbf{Q}^{\dagger}M^{-1}\mathbf{Q} + \mathbf{Q}\cdot V^{\mathrm{ext}} + Q_{\mu}\Phi^{\mu} \qquad (1)$$

with the vector of charges $\mathbf{Q} \equiv \{Q_i\}$, $i = 1, 2, ..., N$, the matrix of capacitances M, and the potential of the electrodes Φ^{μ}, $\mu \in \{+,-,\mathrm{gate}\}$. The external potential is $V^{\mathrm{ext}} = M^{-1}\mathbf{C}_{\mu}\Phi^{\mu}$, where $\mathbf{C}_{\mu}$ is the vector of capacitances between dots and electrodes μ. The microscopic structure of the underlying nanoparticle array appears through the off-diagonal elements of the matrix M, i.e., via the adjacency matrix $A_{ij} = -M_{ij}$ for $i \neq j$. Interparticle charge transport is a stochastic process in which tunneling of an electron between nodes $i \rightarrow j$ at time t is governed by the probability distribution $p_{ij}(t) = \Gamma_{ij}\exp(-\Gamma_{ij}t)$, with the *tunneling rate* $\Gamma_{ij} = -(\Delta E_{ij}/e^2R)/(1 - \exp(\Delta E_{ij}/k_{\mathrm{B}}T))$ determined by the energy change ΔE_{ij} associated with the tunneling process. In our *continuous time* algorithm, the relevant quantities are measured in the following units: $Q[e]$, $V[e/C_g]$, $t[RC_g]$, and $I[e/RC_g]$. More details of the implementation are given in refs 27 and 29. In this paper we focus on the limit $C \ll C_g$. We return to a description of our simulation data below, following a discussion of the experimental results.

Before the transport properties of cellular nanoparticle networks of the type shown in Figures 1 and 2 were examined experimentally, a control sample comprising an assembly with a relatively low void fraction was prepared and measured. The morphology of this control sample is shown in the inset at the top left of Figure 3 and, while there is an appreciable density of voids present in the otherwise close-packed two-dimensional (2D) layer, the overall topology of the nanoparticle array differs dramatically from that of the networks shown in Figures 1, 2, and 4. The sample morphology is, however, similar to that of the disordered arrays studied by Parthasarathy et al.[5]

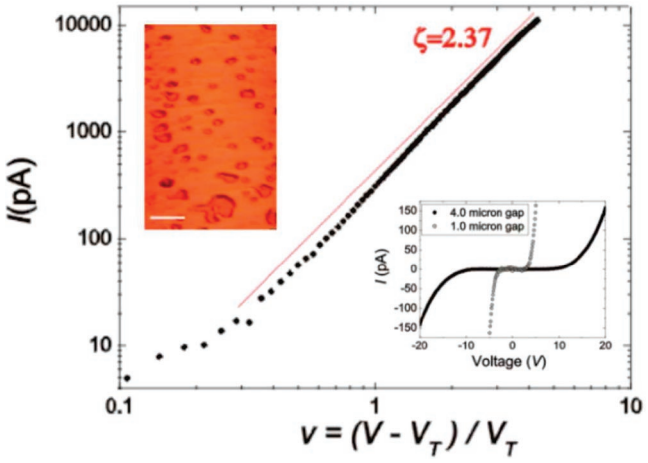

Figure 3. log−log plot of current vs reduced voltage (across a 1 μm electrode gap) for a nanoparticle network with a relatively low void fraction. For values of v above 2, the scaling exponent is 2.37 whereas values closer to 1 (i.e., in the "crossover" region defined by Parthasarathy et al.[5]), are associated with a scaling exponent of ~2.56. The inset at the upper left is an atomic force microscopy (AFM) image of the sample morphology (scale bar: 1 μm) whereas that in the bottom right corner is a plot of the raw $I(V)$ data for 4.0 and 1.0 μm gaps.

$I(V)$ characteristics of the control sample are plotted in the lower right inset to Figure 3 for both a 1 and a 4 μm electrode gap. Figure 3 is a log−log plot (for the 1 μm gap) of current vs reduced voltage, $v = (V - V_{\mathrm{th}})/V_{\mathrm{th}}$, where V_{th} is the threshold voltage (which may be accurately determined[11] from a plot of I dV/dI vs V). For values of $v > 1.6$, the slope of the log−log plot (i.e., the scaling exponent, ζ) is 2.37 ± 0.05, within experimental error of the value of 2.25 ± 0.1 found by Parthasarathy et al.[5] for ordered arrays. We also observe the deviations from single power law behavior reported by the Jaeger group[5,6] for disordered nanoparticle arrays: in Figure 3 the slope of the log−log plot changes from 2.37 (for $v > 1.6$) to 2.56 (± 0.09) for v between 0.6 and 1.6.

Although we attain rather good agreement with the values of ζ measured by Parthasarathy et al.,[5] there are of course two significant differences between the sample geometries in the respective experiments. First, we have deposited the electrodes on the nanoparticle assembly in a rather less controlled fashion—the contacts are not lithographically defined. One might ask whether the precise micro-/nanostructure of the contacts could act as a contribution to the overall disorder of the system and thus affect the measured scaling exponents. It appears from the results of Figure 3 that the mechanism of contact fabrication does not radically change the scaling exponent (at least for moderately disordered systems). Second, and more importantly, the contacts in our experimental geometry are 2 orders of magnitude wider than those used in the work of Parthasarathy et al.[5] (i.e., 200 μm vs 2 μm). As shown by Rendell et al.,[10] however, there is a rather rapid saturation of the value of the scaling (or nonlinearity) exponent as a function of network width. This is because conducting pathways which span a transverse length significantly wider than the contact-to-contact gap make a negligible contribution to the total current.

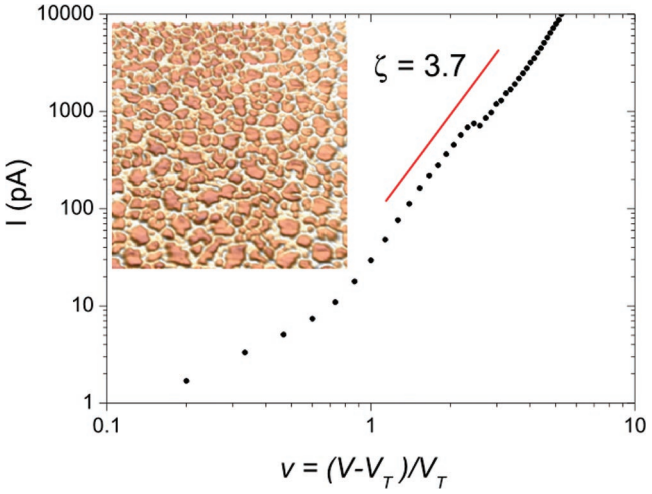

Figure 4. Current−voltage characteristic (log−log plot) of a cellular nanoparticle network measured at 4.5 K across an electrode gap width of 500 nm. The inset is an AFM image ($3 \times 3\ \mu m^2$) of the network. The $I(V)$ curve is associated with an average exponent, ζ of 3.7 ± 0.1.

For nanoparticle arrays having a significantly higher degree of topological complexity, the form of the $I-V$ curve and the scaling exponent differ significantly from those of Figure 3. In the inset to Figure 4 we show an AFM image of a nanoparticle array containing a high density of spatially correlated voids. The voids originate from nucleated solvent dewetting which, due to the coupling between solvent and nanoparticle dynamics described elsewhere,[17,20] ultimately produces what is best described as a cellular network structure. As shown in Figure 4, the $I(V)$ characteristics of networks of this type[30] are associated with scaling exponents substantially larger ($\zeta \sim 4$, see also Figure 7) than those observed by Parthasarathy et al.[5] or predicted by a number of previous simulations of current flow in disordered 2D arrays.[7,8] Although Ancona et al. have previously observed scaling exponents as high as 4 in 2D arrays of thiol-passivated Au nanoparticle, in that work X-ray photoelectron spectroscopy was used to determine nanoparticle (fractional) coverage. Photoemission, based as it is on the average attenuation of a signal from a macroscopic sample area, cannot distinguish between correlated and uncorrelated void distributions.

Of particular importance, therefore, is the question of whether the *correlated* nature of the void distribution[20] strongly affects the scaling exponent. As compared to a void-free array, or indeed a nanoparticle assembly with a random distribution of voids, the spatial correlation of the voids necessarily forces the charge to follow rather tortuous paths from one electrode to the other. To increase the current−voltage dependence from an approximate quadratic relationship (as observed in ordered arrays) to close to a fourth order dependence near threshold, however, requires that within a small voltage increment a relatively higher number of channels "switch on" together for networks of the type we have studied. This in turn raises the issue of the *local* connectivity of the nanoparticle arrays and we return to this point below when discussing the results of the charge transport simulations.

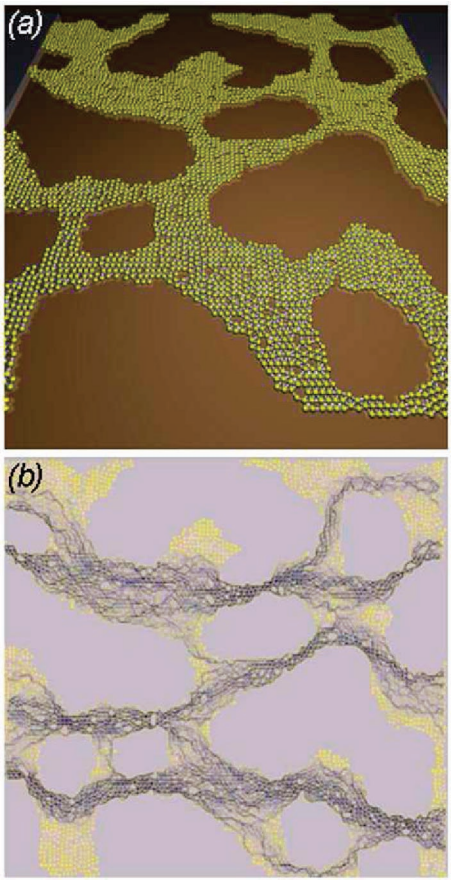

Figure 5. (a) Three-dimensional representation of part of a typical cellular network structure used in the simulations. (b) Simulated charge transport through the network. Electrodes are placed at boundary nodes on the left- and right-hand sides of the structure. Paths of the electron transport are traced throughout the sample where darker colors correspond to a larger flow of electrons.

In Figure 5a we show a three-dimensional representation of the spatial distribution of nanoparticles in a simulated network structure whose morphological characteristics (as measured by Minkowski measures[20]) are very similar to those of the samples studied in our experiments. (Note the higher void density as compared to the simulated network shown in Figure 2.) The calculated charge transport pathways through the network are shown in Figure 5b with simulated current vs reduced voltage curves plotted in Figure 6. In the range of values above threshold a strong nonlinear behavior of the current is found with exponent $\zeta \approx 3.9$, comparable to the experimental results. Note that this result is obtained *without* the imposition of random charge disorder[5,7]—the topology and connectivity of the network alone is enough to produce a scaling exponent in good agreement with experiment. (For comparison, our simulations on void-free nanoparticle arrays with random charge disorder give $\zeta = 2.25$, in excellent agreement with previous experimental and theoretical work.[5] The analytical results for a single dot and a linear $I(V)$ characteristic for a 1D chain of nanoparticles, in addition to a variety of regular arrays, are well-reproduced by the model. Moreover, results for fixed-connectivity cellular networks with scale-free loops can be found in ref 28.)

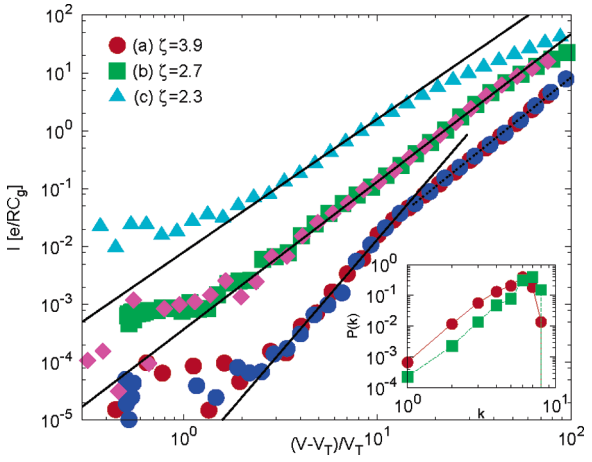

Figure 6. log−log plots of current vs reduced voltage extracted from simulations of charge transport in cellular nanoparticle networks. (a) $I(V)$ characteristic for the network shown in Figure 5. The simulation reproduces the scaling exponent of 4 found in experiment. (b) For the simulated network shown in Figure 2 which has a lower void density. The results of two separate runs are shown in both cases. (c) For comparison, we show the simulated $I(V)$ characteristic of a void free, perfectly ordered nanoparticle array of the type studied by, for example, Parthasarathy et al.[5] Inset: Connectivity distributions of the networks.

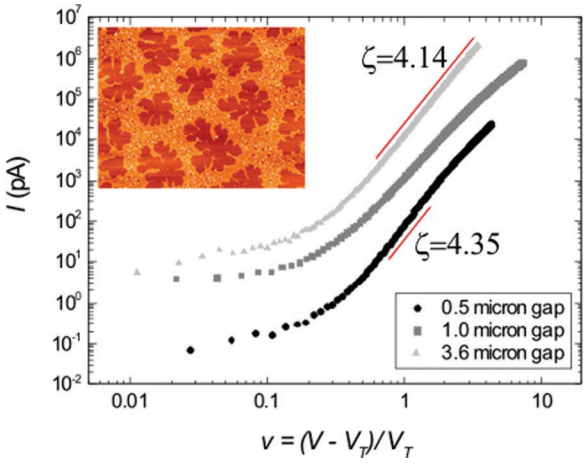

Figure 7. Inset: AFM image (10 μm × 7.8 μm) of a nanoparticle assembly containing both micrometer-scale and nanoscale voids. The $I(V)$ characteristics for the network, taken across a range of gap widths, are shown. The distinct change in slope observed for measurements across a 0.5 μm gap (where ζ "rolls over" from 4.35 for values of v close to 1 to $\zeta = 3.44$ for $v > 2.5$) are washed out for $I(V)$ data acquired across wider gaps. (Note that the $I(V)$ curves for the 1.0 and 3.6 μm gaps are offset by 1 and 2 decades, respectively, for clarity.)

We also show in Figure 6 the $I(V)$ characteristics for the network structure of Figure 2. Here, however, we find a smaller exponent $\zeta = 2.8$, similar to the values found by Parthasarathy et al.[5] for networks with a relatively low void fraction. A key difference between the structure of the simulated networks shown in Figure 2 and Figure 5 is the distribution of nanoparticle connectivity. As shown in the inset to Figure 6, the broader distribution of connectivity for the network shown in Figure 5a yields an exponent with a value close to 4. Narrower distributions of connectivity (such as that associated with the network shown in Figure 2) systematically lead to smaller exponents $\zeta < 3$ (despite having higher mean values of connectivity).

To elucidate the effects of increased levels of network complexity, we measured the $I(V)$ characteristics of a sample comprising nanoscale voids *and* much larger micrometer-scale holes (see Figure 7).[31] Note that the sample in this case comprises two "nested" networks where there is a distinct bimodality in the size of the voids. The larger holes shown in the inset to Figure 7 have a "diameter" of order 2 μm and are surrounded by a smaller scale network containing voids of nanoscale dimensions (similar to those observed in Figure 2). Figure 7 shows the scaling behavior of the $I(V)$ characteristics for this sample (for three different contact gap widths), where the scaling exponent is again ∼4.0. Interestingly, however, for the smallest gap width (500 nm) we observe a slight increase (outside of the experimental error) of the exponent above that of the network shown in Figure 4. However, as the microhole diameters are significantly larger than 500 nm, the sample in this case comprises a set of "patches" of smaller scale network similar to that shown in Figure 2. At the largest gap width, the scaling exponent near threshold is ∼4.1, very similar to that observed for the experimental and simulated single length scale networks discussed above. Hence, it would appear that voids with a correlation length/size of order the electrode gap width have little effect on the transport properties of the nanoparticle array.

There are nevertheless important, albeit subtle, differences in the $I(V)$ characteristics of the dual length scale network shown in Figure 7 as a function of electrode spacing. For the smallest gap width (500 nm), there is a distinct change in the slope of the graph from $\zeta = 4.35$ to $\zeta = 3.44$ as the value of v is increased from a value close to 1 to values greater than ∼2.5. Note that similar changes in slope are observed for the simulated data shown in Figure 6a. With increasing gap width, this "roll off" of the scaling exponent is washed out so that for an electrode spacing of 3.6 μm, the $I(V)$ characteristic recovers close to single power law behavior across a relatively large range of v (see upper curve in Figure 7). It is noteworthy that while the 0.5 and 1.0 μm gaps are associated with log−log $I(V)$ characteristics which display distinct changes in slope, as previously observed and discussed by Parthasarathy et al.[5] and Reichhardt and Olson Reichhardt,[7] the largest gap width over the same voltage range produces current flow which can be fit with a single power law.

In conclusion, we have measured the electrical transport properties of self-organized and topologically complex nanoparticle assemblies. Current flow in these assemblies follows an approximate quartic dependence on the (reduced) bias voltage. Numerical simulations of charge transport, involving modeling of single electron transport through different network morphologies, reproduce the experimental data well and illustrate the importance of the distribution of nanoparticle connectivity in defining the value of ζ. Future work will focus on mapping the *local* charge transport properties of close-packed and cellular nanoparticle lattices using variable temperature scanning probe techniques.

Acknowledgment. We gratefully acknowledge funding from the European Union's Framework 6 Programme: Marie Curie Research Training Networks, Contract MRTN-CT-2004-005728 (PATTERNS). B.T. acknowledges program P1-0044 (Slovenia) for funding. The U.K. Engineering and Physical Sciences Research Council (EPSRC) also funded M.O.B. and C.P.M. for the duration of this work. We thank the members of the PATTERNS network for helpful discussions regarding pattern formation in nanoparticle assemblies including, in particular, Uwe Thiele, Ulli Steiner, James Sharp, and Mathias Brust. In addition, we thank Bryan Gallagher and Laurence Eaves for providing access to the cryostats used in this work.

References

(1) Lin, X.-M.; Jaeger, H. M.; Sorensen, C. M.; Klabunde, K. J. *J. Phys. Chem. B* **2001**, *105*, 3353.
(2) Bigioni, T. P.; Lin, X.-M.; Nguyen, T. T.; Corwin, E. I.; Witten, T. A.; Jaeger, H. M. *Nat. Mater.* **2006**, *5*, 265.
(3) Narayanan, S.; Wang, J.; Lin, X.-M. *Phys. Rev. Lett.* **2004**, *93*, 135503.
(4) Huang, J.; Kim, F.; Tao, A. R.; Connor, S.; Yang, P. *Nat. Mater.* **2005**, *4*, 896.
(5) Parthasarathy, R.; Lin, X.-M.; Jaeger, H. M. *Phys. Rev. Lett.* **2001**, *87*, 186807.
(6) Parthasarathy, R.; Lin, X.-M.; Elteto, K.; Rosenbaum, T. F.; Jaeger, H. M. *Phys. Rev. Lett.* **2004**, *92*, 076801.
(7) Reichhardt, C.; Olson Reichhardt, C. J. *Phys. Rev. Lett.* **2003**, *90* 046802.
(8) Reichhardt, C.; Olson Reichhardt, C. J. *Phys. Rev. B* **2003**, *68*, 165305.
(9) Ancona, M. G.; Kruppa, W.; Rendell, R. W.; Snow, A. W.; Park, D.; Boos, J. B. *Phys. Rev. B* **2001**, *64*, 033408.
(10) Rendell, R. W.; Ancona, M. G.; Kruppa, W. *IEEE Trans. Nanotechnol.* **2003**, *2*, 75.
(11) Ancona, M. G.; Kooi, S. E.; Kruppa, W.; Snow, A. W.; Foos, E. E.; Whitman, L. J.; Park, D.; Shirley, L. *Nano Lett.* **2003**, *3*, 135.
(12) Elteto, K.; Antonyan, E. G.; Nguyen, T. T.; Jaeger, H. M. *Phys. Rev. B* **2005**, *71*, 064206.
(13) Elteto, K.; Lin, X.-M.; Jaeger, H. M. *Phys. Rev. B* **2005**, *71*, 205412.
(14) Middleton, A. A.; Wingreen, N. S. *Phys. Rev. Lett.* **1993**, *71*, 3198.
(15) Maillard, M.; Motte, M. L.; Ngo, A. T.; Pileni, M. P. *J. Phys. Chem. B* **2000**, *104*, 11871.
(16) Pileni, M. *J. Phys. Chem. B* **2001**, *105*, 3358.
(17) Rabani, E.; Reichman, D. R.; Geissler, P. L. Brus, L. E. *Nature* **2003**, *426*, 271.
(18) Ge, G.; Brus, L. *J. Phys. Chem. B* **2000**, *104*, 9573.
(19) Moriarty, P.; Taylor, M. D. R.; Brust, M. *Phys. Rev. Lett* **2002**, *89* 248303.
(20) Martin, C. P.; Blunt, M. O.; Moriarty, P. *Nano Lett.* **2004**, *4*, 2389.
(21) Blunt, M. O.; Martin, C. P.; Ahola-Tuomi, M.; Pauliac-Vaujour, E.; Sharp, P.; Nativo, P.; Brust, M.; Moriarty, P. *Nat. Nanotechnol.*, advance online publication, February 18, 2007 (doi:10.1038/nnano.2007.25).
(22) Schaeffer, E.; Thurn-Albrecht, T.; Russell, T. P.; Steiner, U. *Nature* **2000**, *403*, 874.
(23) Morariu, M. D.; Voicu, N. E.; Schaeffer, E.; Lin, Z.; Russell, T. P.; Steiner, U. *Nat. Mater.* **2003**, *2*, 48.
(24) Brust, M.; Walker, M.; Bethell, D.; Schiffrin, D. J.; Whyman, R. *J. Chem. Soc., Chem. Commun.* **1994**, *7*, 801.
(25) Pauliac-Vaujour, E.; Blunt, M. O; Martin, C. P.; Vancea, I.; Thiele, U.; Moriarty, P. Unpublished.
(26) Martin, C. P.; Blunt, M. O.; Pauliac-Vaujour, E.; Vancea, I.; Thiele, U.; Moriarty, P. Organising Nanoparticles via Directed Solvent Dewetting. Unpublished.
(27) Suvakov, M.; Tadic, B. Simulations of the electron tunneling paths in networks of nanoparticle films. To appear in Lecture Notes of Computer Science, Proceedings of ICCS 2007, Bejing, China.
(28) Suvakov, M.; Tadic, B. Transport processes on homogeneous planar graphs with scale-free loops. *Physica A* **2006**, *372*, 354−361.
(29) Suvakov, M.; Tadic, B. Paper in preparation.
(30) We note that acquisition of $I(V)$ curves from cellular nanoparticle networks of the type shown in Figure 1 and Figure 4 is far from straightforward. A considerable number of samples (particularly those with relatively high electrode gap widths ($\gtrsim 3\ \mu$m)) were open-circuit due to an absence of a sufficient number of percolating pathways across the network.
(31) It is outside the scope of this short paper to discuss in detail the origin of the multilevel organisation shown in the inset to Figure 7. The origin of the voids and the fingering structures[32,33] observed in the micrometer-scale holes will be covered in a future publication.[25]
(32) O'Shea, J. N.; Phillips, M. A.; Taylor, M. D. R.; Moriarty, P.; Brust, M.; Dhanak, V. R. *Appl. Phys. Lett.* **2002**, *81*, 5039.
(33) Yosef, G.; Rabani, E. *J. Phys. Chem. B* **2006**, *110* 20965.

NL061656E